Advances in
Bridge Engineering

ORIGINAL INNOVATION Open Access

Railway bridge damage detection based on extraction of instantaneous frequency by Wavelet Synchrosqueezed Transform

Neda Mostafa*, Dario Di Maio, Richard Loendersloot and Tiedo Tinga

*Correspondence:
n.mostafa@utwente.nl

Department of Engineering Technology, University of Twente, Enschede, The Netherlands

Abstract

In bridge structural health monitoring, typically the dynamic response of the system is used to assess the health condition of the bridge. However, the dynamic interaction between a bridge and a passing vehicle imposes non-stationarity on the system response, whereby the bridge modal parameters become time-dependent and detecting damage, for example, based on the bridge modal parameters, becomes challenging. Dynamic vehicle-bridge interaction (VBI) responses have mainly been investigated for damage detection through identifying signal singularities and abrupt changes. The singularities are usually associated with high-frequency components (relative to the bridge natural frequencies), and it is demanding to isolate the damage-induced singularities from those caused by either an operational condition, i.e., track irregularities, or noise. Unlike the high-frequency range, the influence of damage on the resonance frequency of the coupled system has not been fully explored. The present study proposes the shape of the bridge instantaneous frequency as a damage sensitive feature in which the influence of the vehicle dynamics can be excluded. This study demonstrates the feasibility of a damage detection approach based on the bridge instantaneous frequency by applying Wavelet Synchrosqueezed Transform (WSST). In this approach the bridge instantaneous frequency variation induced by damage is distinguished from the bridge instantaneous frequency variation induced by the vehicle. Several damage scenarios that are implemented numerically are analyzed to verify the method's performance. The results demonstrate that a high resolution instantaneous frequency extracted from the VBI dynamic response outperforms the resonance frequency in determining the local disruption, leading to detecting the damage. A Damage Index (DI) is also proposed as an attempt to quantify the damage severity.

Keywords: Damage detection, Bridge health monitoring, Time-frequency analysis, Non-stationary response, Instantaneous frequency, VBI acceleration response

1 Introduction

Structural Health Monitoring (SHM) systems aim at identifying damage to assess the structural integrity and safety of a structure. Moreover, the obtained damage information can serve as an input for Bridge Management Systems (BMSs) to guide and manage the maintenance activities during the service life of bridges. An SHM system can provide

information at different levels regarding the condition of a bridge where the primary level is detecting damage. Several techniques have been developed for damage detection in bridges. The majority can be grouped into four categories. The first group involves model-based techniques, which are based on updating the parameters of an analytical or numerical model such that the model matches the real measurements (Friswell 2007; Farahani and Penumadu 2016; Li et al. 2013). However, these techniques are not always efficient because the bridges are massive structures with a complex geometry. Moreover, the accuracy of the results is dependent on the accuracy of the developed model. The second group contains the data-driven methods (DDMs) that are not supported by physical models such as neural network (Li et al. 2020; Sun et al. 2020), machine learning (Malekjafarian et al. 2019), feature extraction and pattern recognition (Silva et al. 2016; Comanducci et al. 2016; Santos et al. 2017; Babajanian Bisheh et al. 2020) techniques. The third group which is the traditional approach, contains the modal-based damage detection techniques (Doebling et al. 1998; Moughty and Casas 2017) based on extracting and monitoring the modal properties, which can vary due to the presence of damage. The fourth group contains structural health monitoring techniques based on time-frequency analysis of the Vehicle-Bridge interaction (VBI) response. The current study proposes a damage detection approach based on the instantaneous and natural frequency of the bridge extracted from the bridge forced and free vibration response, respectively. Therefore, the following literature review is on the last two groups where the bridge vibration, free or forced, has been utilized for damage detection.

The standard technique for modal identification is Modal Analysis (MA). Input-output methods or Experimental Modal Analysis (EMA) techniques involve applying a known input, such as a Dirac impulse load, to the structure and measuring the vibration response. To create a desired forcing function, devices such as impact hammers, shakers, or drop weights are required (Dilena et al. 2015). However, they are not efficient and applicable for a bridge in regular operation. Then the Output-only Modal Analysis (OMA) is adopted for a system stationary output while the unmeasured input can be considered as white noise (Rainieri and Fabbrocino 2014). Hence, the response of the structure to an ambient excitation such as wind load or its free vibration due to a passing vehicle is suitable for OMA (Zhang and Brincker 2005; Ojeda 2012; Chang and Kim 2016). Ambient vibration is generally of small magnitude, which cannot be helpful for all bridges (Cantero et al. 2016). Since EMA and OMA are not efficiently applicable for all bridges, railway bridges are generally monitored by extracting the bridge dynamic properties through the free vibration response, which occurs once a passing train has just left the bridge (Cantero et al. 2016). However, the extracted modal parameters, using the bridge free vibrations, before and after the damage occurrence are global and averaged features that may not be sensitive to damage as a local event (Chen 2009). Most damage detection researches have shown that a discontinuity appears in the forced vibration signal when the moving load crosses over damage (Gonzalez and Hester 2013; Meredith et al. 2012; Hester and Gonzalez 2012; Roveri and Carcaterra 2012; Aied et al. 2016), so the forced vibration response may be more sensitive to damage than the free vibration. The VBI response that refers to the coupled dynamic response of a bridge and a moving vehicle has been widely studied in the literature for damage detection in bridges by analyzing the bridge response (*direct methods*) or the vehicle response (*indirect methods*).

VBI has also been applied for Moving Force Identification (MFI) from a vehicle response or a bridge response (Obrien et al. 2015; Obrien et al. 2014). A general overview of MFI techniques can be found in (Yu and Chan 2007).

To narrow down, the scope of the current study is damage detection techniques for bridges that analyze the VBI response measured on the bridge (*direct methods*). In order to position the current study among existing techniques in scope, Table 1 summarizes these studies. Each approach is presented via five attributes: 1) the considered signal, 2) the damage sensitive feature (DSF), 3) the applied signal processing method, 4) the way the vehicle dynamics are simulated and, 5) the validation approach. In the following, some of the attributes ar discussed to distinguish the proposed method.

Regarding the considered signal, Table 1 shows that the bridge time-deflection response (typically taken at the mid-span location) has been mostly used. However, there are motivations to study the bridge acceleration rather than the deflection signal. Firstly, it might not be possible to measure the bridge deflection signal at mid-span directly.

Table 1 An overview of recent damage detection approaches

Research study	Considered response [1]	Damage Sensitive Feature [2]	Applied technique [3]	Moving object	Validation
Huseynov et al. (2020)	$\ddot{x}$	rotation	rotation influence line	series of constant forces	Numerically experimentally
Zhang et al. (2017)	$x, \dot{x}, \ddot{x}$	phase trajectory	low-pass filter & moving average	constant force & mass	Numerically experimentally
He and Zhu (2016)	x	moving frequency	DWT	constant force & vehicle	Numerically
Aied et al. (2016)	$\ddot{x}$	discontinuity in IMF	EEMD	a constant force	Numerically
Yu et al. (2016)	x	Wavelet coefficient	CWT	a constant force	Numerically experimentally
Nguyen (2013)	x	instantaneous frequency	CWT	a half-vehicle	Numerically
Gonzales and Hester (2013)	$\ddot{x}$	mid-span 'static' deflection and acceleration	MAF	a constant force & a vehicle	Numerically
Khorram et al. (2013)	x	Wavelet coefficients	CWT & Factorial Design	a constant force	Numerically
Zhang et al. (2013)	$\dot{x}$	wavelet coefficient	CWT	a constant force	Numerically
Hester and Gonzalez (2012)	$\ddot{x}$	wavelet coefficient	CWT	a constant force	Numerically
Meredith et al. (2012)	$\ddot{x}$	high peaks in IMFs	MAF followed by EMD	a constant force	Numerically
Roveri and Carcaterra (2012)	x	instantaneous frequency	HHT	constant force	Numerically
Pakrashi et al. (2009)	ε	Wavelet coefficient & Wavelet phase	CWT	vehicle	Numerically experimentally
Zhu and Law (2006)	x	Wavelet coefficient	CWT	constant force	Numerically

[1] $x, \dot{x}, \ddot{x}$ and ε represent the bridge displacement, velocity, acceleration and strain response.

[2] IMF: Intrinsic Mode Function.

[3] DWT: Descrete Wavelet Transform, CWT: Continouse Wavelet Transform, EMD: Empirical Mode Decomposition, EEMD: Ensemble Empirical Mode Decomposition, MAF: Moving Average Filter, HHT: Hilbert Huang Transform

Secondly, in comparison with the deflection signal, the bridge acceleration signal is more sensitive to damage (Hester and Gonzalez 2012). The acceleration signal contains more information about damage as well as noise, making it challenging but also valuable to analyze. Therefore, measuring the bridge acceleration is considered more practical than measuring the bridge deflection.

Regarding the applied technique Table 1 shows that Empirical Mode Decomposition (EMD) (Meredith et al. 2012) and Ensemble Empirical Mode Decomposition (EEMD) (Aied et al. 2016) were applied to the acceleration response of the damaged bridge models induced by a constant moving force. They aimed to capture the singularities that appeared in a series of Intrinsic Mode Functions (IMFs) corresponding to high-frequency components. Table 1 further shows that Continuous Wavelet Transform (CWT) is one of the most applied methods, since the basic principle of the wavelet-based damage detection techniques is detecting singularities, and abrupt changes (Pakrashi et al. 2007). Hester and Gonzalez (2012) applied CWT to a modeled bridge acceleration response and concluded that in the coefficient matrix, the damaged strips have a higher energy content than the healthy strips if the frequencies are distant from the natural frequencies. Later, they (Gonzalez and Hester 2013) assumed that the damage was already detected, and they investigated how a singularity changes with damage location and severity. Regardless of the applied method, a commonality among the above methods is the DSF is based on singularities that appear in the response of a damaged structure, but do not exist in its healthy response (Gonzalez and Hester 2013). The singularities are usually associated with high-frequency components (in comparison with the bridge natural frequencies), and it is demanding to isolate the damage-induced singularities from those caused by either an operational condition (track irregularities) (Zhai and Sun 2008) or noise (Zhang et al. 2017). This might be a reason why they are efficient for simulated signals or laboratory experiments but not for field applications.

Moreover, in most of the above studies, the vehicle is mainly modeled as a constant force, whereas the vehicle-bridge dynamic interactions are completely excluded. Those studies that utilized vehicle models did not explicitly investigate the influence of the vehicle on the system response and the damage detection approach. In general, a moving force model is suitable for the cases where either the weight of the vehicle is much smaller than the bridge or the effect of the dynamic behavior of the vehicle is not of interest (Zhai et al. 2019). For trains, it is known that the train weight is not negligible and the trains thus affects the dynamic properties of the VBI system (He et al. 2011). Therefore, for the current study, the vehicle is modeled as a point mass to include the influence of the vehicle mass on the system dynamics response.

To overcome the limitations as mentioned above, the feasibility of a damage detection concept based on the following axioms will be studied;

- The bridge free vibration mainly reflects the global dynamics properties, which may overshadow a small and local variation triggered by the passing vehicle and captured by the vehicle-bridge coupled dynamic response.
- A damage-induced singularity originates from a sudden stiffness change between two bridge elements once the vehicle passes over a damaged element. This sudden stiffness change causes a deviation in the time-dependent resonance of the system.

- A passing vehicle, depending on its (dynamic) properties, can affect the bridge resonance frequencies. Thus, upfront the damage investigation, the bridge forced and free vibrations are required to identify their frequency difference in a healthy state.
- The vehicle is modeled as a point mass to impose the bridge resonance frequency change due to the operational condition (i.e. added mass) as occurs in practice.
- a high-resolution time-frequency analysis technique is required to extract the VBI system's time-dependent resonances as accurately as possible. Wavelet SynchroSqueezed Transform (WSST) is used for the current study as its performance has been investigated and validated (Mostafa et al. 2021).

The following section will explain the methodology in three steps: 1) phase separation, 2) frequency extraction and, 3) frequency analysis. A numerical model has been used to validated the complete damage detection approach, which is presented in Section 2. The results are discussed in Section 4, and the final section provides the conclusions. It is worth mentioning that a large amount of vibration data of a real bridge, the Boyne viaduct is available. The bridge condition is considered healthy due to recent refurbishment activities. Therefore, the first two steps, the phase separation and the frequency extraction, have been verified with the field measurement data of the Boyne viaduct.

2 Methodology

Generally, a bridge vibration response due to a passing train contains three phases: 1) the entrance phase, 2) the traverse phase, and 3) the leaving phase. The entrance phase covers the period right before the train enters the bridge, and the part of the vibration signal associated with this phase is not investigated in this paper. The traverse phase is the period that the train is either partly or entirely on the bridge, and the leaving phase is the period right after the train has left the bridge. The traverse and the leaving phase correspond to the bridge forced and free vibrations, respectively. The traverse phase is known as the vehicle-bridge interaction response (VBI), representing the response of the coupled system of both bridge and vehicle.

The flowchart of the conventional damage detection technique based on monitoring the variation of the bridge natural frequency is presented in Fig. 1 where f_b and f_m are the baseline and the measured bridge natural frequency extracted from the leaving phase response.

It is known that a discontinuity emerges in the response when the moving mass crosses a damaged element. Both the traverse and the leaving phase signals contain local and global information. However, the global properties dominate in the leaving phase, whereby slight variations induced by damage may be overshadowed. Therefore, the traverse phase is believed to be more sensitive to damage than the free vibration response. The flowchart of the proposed concept presented in Fig. 2 shows that the proposed method extends the traditional method by including both the traverse phase and the leaving phase response and accordingly utilizing the bridge instantaneous and natural frequency respectively.

The challenge of utilizing the traverse phase response is that the traverse phase, in addition to damage, is also sensitive to the operational conditions. Therefore, the proposed algorithm for a VBI system starts by setting a baseline instantaneous frequency

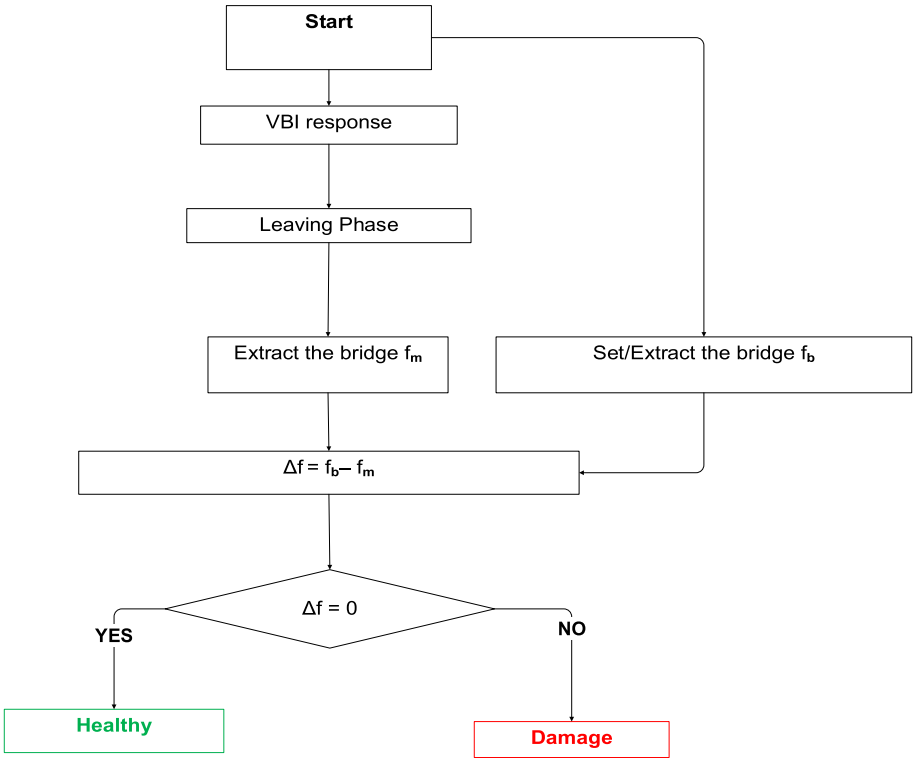

Fig. 1 The flowcharts of the damage detection techniques based on the bridge natural frequency extracted from the leaving phase

extracted from the bridge traverse phase, $\mathcal{F}_b$ for a passing vehicle type. If different types of trains pass the bridge, a train type should be defined as the target vehicle to set $\mathcal{F}_b$. A parallel study is investigating the definition of the target vehicle type, which is out of the scope of the current study. The traverse phase provides a baseline for a healthy bridge. An instantaneous frequency extracted from a measured traverse phase response, $\mathcal{F}_m$, can then differ from $\mathcal{F}_b$ due to; 1) a variation of the operational conditions or 2) the presence of damage. Therefore, the source of the instantaneous frequency difference must be identified first. The shape correlation ρ and the magnitude variation δ are proposed to identify the source of $\mathcal{F}_b$ variation. If the difference is caused by damage, then δ can be used as damage index. The proposed damage index is an attempt to quantify damage severity. Moreover, the local baseline deviation around the damage location shows the potential of the proposed method for damage localization. However, the focus of the current study is on detecting damage. Damage localization and damage quantification are out of the scope of the current study. The proposed concept is presented in three analysis steps; 1) phase separation, 2) frequency extraction, 3) frequency analysis.

2.1 Phase separation

Phase separation refers to splitting the entire response into the entrance, traverse, and leaving Phase responses. As these phases represent different systems with different dynamics properties, the phase separation step is of paramount importance. Even though phase separation is relatively straightforward, it is a foundational block of the

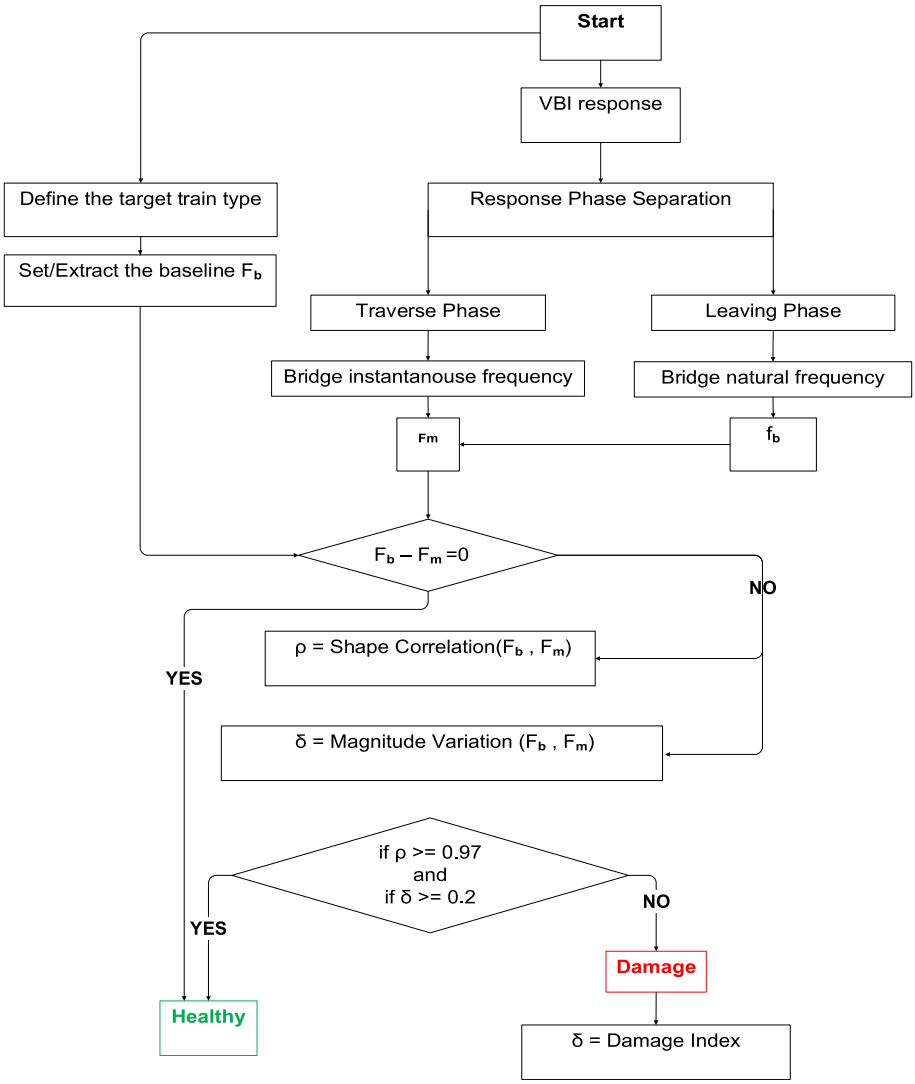

Fig. 2 The flowcharts of the damage detection techniques based on the VBI system instantaneous frequency extracted from the traverse phase

proposed concept. The phase separation step is performed based on the position of a train on the bridge, see Fig. 3.

The traverse phase starts when the first wheel set of the train enters and ends when the last wheel set leaves the bridge. This phase describes the forced response of the bridge due to the moving train, including the train-bridge dynamic interaction. The leaving phase is the free vibration of the bridge. Figure 3 shows a schematic view of the phase separation for a sample signal. This signal was measured by an accelerometer installed at mid-span of the Boyne viaduct in Ireland (Connolly et al. 2017). It can be seen that there is no visible sign in the time signal on when the train enters or leaves the bridge meaning that the phase separation is not straightforward for field data. The exact moments of the entrance and exit of the train can be identified by knowing the train velocity and the location of the accelerometer. The train velocity calculation can be carried out in several ways. In this study, it is obtained from the driving frequency, $f_{dr}=V_{vehicle}/L_{bridge}$ which is

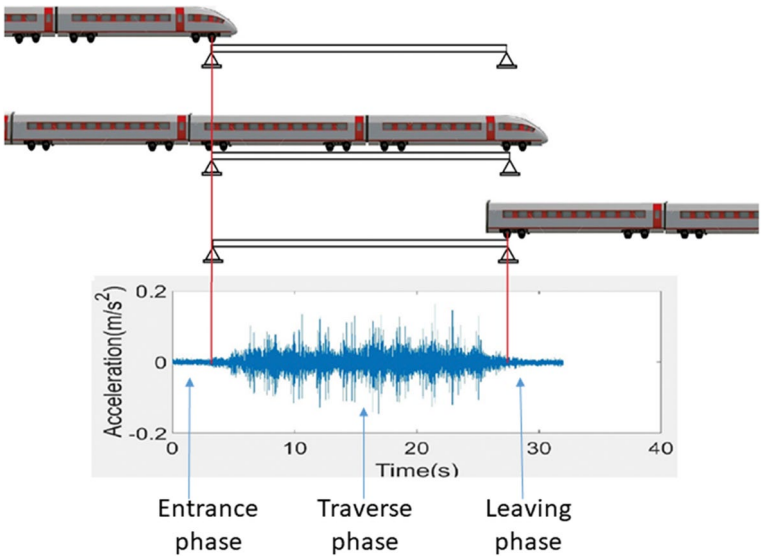

Fig. 3 Schematic view of the phase separation

present in the frequency content of the bridge dynamic response (Lu et al. 2012). The driving frequency is the inverse of the time that a train with a velocity V needs to pass a bridge with a length of L. By extracting the driving frequency for a bridge with a known length, the average vehicle velocity can be calculated.

2.2 Frequency extraction

The most challenging step of this methodology is the frequency extraction. Although the traverse and the leaving phase both contain the bridge response, they represent different systems. The traverse phase contains the response of the vehicle-bridge coupled system where the time-dependent mass distribution on the bridge leads to a time-variant system, whereas the leaving phase, as the bridge free vibration, represents a time-invariant system. In other words, the dominant frequency components of the leaving phase are the bridge natural frequencies, whereas the traverse phase contains the time-dependent frequency components that originate from the bridge, the vehicle, and the track vibration. The first challenge of the time-frequency analysis of the traverse phase, knowing that a VBI response contains closely-spaced spectral components due to the vehicle-bridge dynamic coupling (Connolly et al. 2015), is to distinguish the bridge resonance from other resonances. A reliable and efficient approach is first to extract the bridge natural frequency from the leaving phase and then trace it back in the traverse phase. The bridge natural frequency extracted from the leaving phase is used as the reference to trace the VBI system time-dependent resonance corresponding to the bridge natural frequency. Including both the traverse and the leaving phase response and analyzing them individually as two separate systems is an essential base of the proposed concept to distinguish the bridge resonances from the system resonances.

The second challenge of the time-frequency analysis of the traverse phase is to extract the time-dependent resonance of the bridge as accurate as possible. A high-resolution and sharp time-frequency representation may reflect more information about a local

signal disruption than a low-resolution or blurry time-frequency representation. Therefore, a high resolution time-frequency method is required to extract the instantaneous frequencies of the vehicle-bridge interaction response. The performance of Empirical Mode Decomposition (EMD), Local Mean Decomposition (LMD), The Continuous Wavelet Transform (CWT) and the Wavelet SynchroSqueezed Transform (WSST) has been investigated and it has been concluded that among the aforementioned methods WSST can separate the time-dependent resonances of the VBI system and capture the time-dependent variation of the resonances of the system without the prerequisite for the signal to be mono-component (Mostafa et al. 2021). Moreover, the performance of WSST has been validated for the field data of Boyne bridge in previous work of the authors (Mostafa et al. 2021). In the following WSST is presented briefly.

The continuous wavelet transforms the one-dimensional time signal $x(t)$ into a two-dimensional quantity, $W(a,b)$, where a and b are the translation and the scale variables respectively and the function ψ is called the 'mother' wavelet.

$$W_x(a,b) = \int x(t) a^{-1/2} \psi\left(\frac{t-a}{b}\right) \tag{1}$$

However, the time frequency representation is somewhat blurred since $W(a,b)$ is spread out over a region around a on the time-scale (Daubechies and Maes 1996). Daubechies and Maes (1996) observed during the time-frequency analysis of audio signals for speaker identification that, the oscillatory behavior of the signal at time b indicates the original frequency ω, despite the fact that $W(a,b)$ is smeared out in a (scale), regardless of the amplitude of a. The process of synchrosqueezing tries to make the resulting time-scale image of CWT more precise.

In summary, WSST (Daubechies et al. 2011) has three steps. Step one is calculating the continuous wavelet transform of a time signal, $x(t)$ by Eq. 1. Step two is calculating the instantaneous frequency by:

$$\omega_x(a,b) = \frac{\frac{\partial W_x(a,b)}{\partial b}}{2\pi i W_x(a,b)} \tag{2}$$

where the frequency variable ω_x and the scale variable a are binned and computed only at discrete values a_k, with $a_k - a_{k-1} = (\Delta a)_k$. The third step is to re-assign the scale variable a to the frequency variable ω by calculating the Synchrosqueezed transform, T_x as:

$$T_x(\omega_l, b) = (\Delta\omega)^{-1} \sum_{a_k} W(a_k, b) a_k^{-3/2} (\Delta a)_k \tag{3}$$

The transform function $T_x(\omega_l b)$ is determined over time, only at the centers ω_l of the subsequent bins $\left[\omega_l - \frac{1}{2}\Delta\omega, \omega_l + \frac{1}{2}\Delta\omega\right]$, with $\Delta\omega = \omega_l - \omega_{l-1}$.

2.3 Frequency analysis

The extracted instantaneous frequency from the traverse phase provides a baseline for a healthy bridge. The bridge instantaneous frequency extracted from a measured response can deviate from the baseline due to variation of the operational conditions or due to the presence of damage. It is worth noting that the frequency variation due to the seasonal effect is not investigated in this study. The operational conditions are commonly considered

to be the length, mass, and velocity of the vehicles. For the current study, however, only the vehicle's mass is investigated as a variable operational condition since its influence on the bridge frequency is well known. Although the vehicle's mass and the damage can both affect the traverse phase response, their impacts are on different scales. The operational condition affects the bridge instantaneous frequency globally, whereas the damage imposes a local variation in the bridge instantaneous frequency. Once the moving mass crosses a damaged section with a lower stiffness, a discontinuity appears in the response. This local discontinuity causes the instantaneous frequency deviation. The proposed damage detection method is based on the deviation of the baseline instantaneous frequency ($\mathcal{F}_b$) by calculating two features; 1) the baseline shape correlation, ρ and, 2) the magnitude variation, δ. In statistics, the Pearson correlation coefficient calculates a linear correlation measure between two data sets. The baseline shape correlation calculates the global shape correlation between a measured instantaneous frequency ($\mathcal{F}_m$) and the baseline instantaneous frequency ($\mathcal{F}_b$).

$$\rho(\mathcal{F}_b, \mathcal{F}_m) = \frac{1}{n-1} \sum_{i=1}^{n} \left(\frac{\mathcal{F}_{b,i} - \mu_{\mathcal{F}_b}}{\sigma_{\mathcal{F}_b}} \right) \left(\frac{\mathcal{F}_{m,i} - \mu_{\mathcal{F}_m}}{\sigma_{\mathcal{F}_m}} \right) \tag{4}$$

where μ and σ are the mean and standard deviation of the instantaneous frequency as a time series with n samples (Kirch 2008). A low correlation coefficient suggests a considerable difference in shape and therefore, a local variation of the bridge instantaneous frequency, which can indicate damage. On the contrary, a change in operational or environmental conditions can also lead to a change in the response, but this will be a more global change which leads to a high correlation coefficient. However, a small amount of damage may not lead to a low correlation coefficients. Therefore, the magnitude variation, as the second feature, is introduced to quantify the deviation of the measured instantaneous frequency, $\mathcal{F}_m$ from the baseline instantaneous frequency, $\mathcal{F}_b$.

$$\delta(\mathcal{F}_b, \mathcal{F}_m) = \frac{\sum_{i=1}^{n-1} \left[(\mathcal{F}_{b,i} + \mathcal{F}_{b,i+1}) - (\mathcal{F}_{m,i} + \mathcal{F}_{m,i+1}) \right]}{\sum_{i=1}^{n-1} \left[(\mathcal{F}_{b,i} + \mathcal{F}_{b,i+1}) - 2f_b \right]} \tag{5}$$

where f_b refers to the bridge fundamental frequency, which is constant in time and a scalar value. Whereas the instantaneous frequency of the traverse phase yields a curve indicating that the bridge resonance continuously changes in time depending on the location of the moving mass. The denominator of Eq. 5 calculates the area bounded by $\mathcal{F}_b$ and f_b for the intact bridge. It, therefore, corresponds to the variation of the baseline instantaneous frequency of the intact bridge induced by the operational condition. Once the instantaneous frequency of a measured response differs from the baseline, which would be the case when damage is present, then the bounded area between $\mathcal{F}_b$ and $\mathcal{F}_m$ is a nonzero value that quantifies the magnitude variation and it can be a negative or positive value.

3 Numerical model

Although a large amount of vibration data is available for the Boyne bridge, the measurements are not applicable for the validation of the proposed damage detection approach, as recent refurbishments have removed all damage that was potentially present. Hence, to verify the proposed approach, a bridge is modeled numerically.

All finite element simulations are conducted in two-dimensional space in ABAQUS where the analysis scheme is chosen to be the Newmark implicit time integration, assuming an average acceleration during each time step. Linear Timoshenko beam elements were used. The bridge model (the center part of 50 m) has 200 beam elements of 1 m thickness and 0.5 m width with Young's modulus of E=210 GPa, density of ρ=7860 kg/m^3. The fundamental frequency of the bridge model is 2.1 Hz. According to Eurocode EN 1991-2 (2003) the bridge fundamental frequencies for a span length between 20-100 m are in the range 1.7-4 Hz. The bridge model parameters are adopted from (Zhu and Law 2006; Mahmoud 2001) where the bridge length and its fundamental frequency are in the acceptable range. Damping is modeled by implementing Rayleigh damping with the coefficients of α=0.001 and β=0.001. The benchmark simulation corresponds to a point mass equal to 10% of the bridge mass which slides with a speed of 5 m/s over the bridge. The mass slides through a node to surface interaction, while a hard contact model is used (Saleeb and Kumar 2011).

The bridge model is modified to obtain the bridge free vibration, while the mass is not present on the bridge. To this end, an approaching and leaving length are added before and after the bridge to properly locate the mass during the forced and free vibration phases. The length of the approaching and the leaving parts are 25m and both are modelled with beam elements that are clamped in all their nodes. The approaching part is not strictly necessary, but it is used to provide symmetry to the structure.

To calculate the bridge acceleration, three dynamic analysis steps are implemented, corresponding to the mass approaching, crossing and leaving the bridge, representing the entrance, traverse and the leaving phase displayed in Fig. 3.

The stiffness (or equivalently the elastic modulus E) of the elements at the damage location is reduced (Zhang et al. 2017) to implement damage on the bridge. The locations $L/2$ and $3L/4$ are selected to introduce the damage. Two types of damage with different severity are investigated based on the assessment of Boyne viaduct as a case study (Connolly et al. 2017). For the first type, damage grows locally, similar to pitting corrosion or a loose connection. This phenomenon is implemented by reducing the stiffness of a single element. For the second type, the damage propagates along the elements, similar to general corrosion. This damage is implemented by reducing the stiffness of multiple elements around the damage location (Fig. 4).

In addition to the baseline simulation, four groups of simulations are executed to verify the proposed approach for various operational conditions and health states. In the first group, moving masses equal to 5%, 15%, 20%, and 25% of the bridge mass are used, and the bridge is considered healthy. In the second group, local damage is implemented with different severities at location $L/2$ (mid-span). In the third group, the location of the

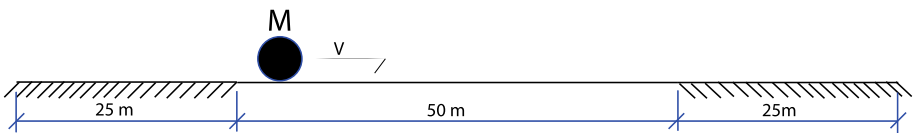

Fig. 4 Schematic of the numerical model, showing the 50 m span and 25 m approaching and leaving sections

damage is moved to $3L/4$. Group four is implemented to investigate propagated damage around the bridge mid-span. Table 2 provides an overview of the four groups of simulations that aim at investigating the sensitivity and performance of the proposed damage detection approach for various VBI system states.

4 Results and discussion

4.1 Baseline simulation

The bridge forced, and free vibration responses are calculated using the proposed VBI model according to the baseline simulation in Table 2. The first Eigen frequency of the bridge model obtained in Abaqus is 2.1 Hz. This frequency matches well with the analytical value of 2.08. Moreover, to verify WSST, as the accuracy of the applied technique, the bridge frequency extracted from the leaving phase by applying WSST is equal to 2.1 Hz, which is well matched with the analytical value.

Figure 5 shows the simulated VBI system response evaluated at the bridge mid-span for the baseline simulation.

The moving mass induces non-stationarity into the signal, meaning that the bridge fundamental frequency changes in time. The bridge frequency variation is not visible in the time signal, since the variation is small. The figure looks very similar to a typical field measurement on a bridge where the level of the bridge acceleration and also the noise during the traverse phase are higher than in the leaving phase. The high frequency component appearing in the traverse phase is an artificial effect of the numerical simulation that corresponds to the inverse of the time taken by the mass for passing a numerical grid. This effect does not exist in the field data. However, usually bridge vibration field data looks noisy due to the vibration traces of the train and the track components. The

Table 2 The healthy and damage scenarios that have been investigated numerically

Test case	Vehicle-bridge mass ratio (%)	Stiffness reduction (%)	Damaged element (No.)
Baseline simulation			
1	10	-	-
Variable operational condition			
2	5	-	-
3	15	-	-
4	20	-	-
5	25	-	-
Damage type 1 at L/2			
6	10	30	1
7	10	50	1
8	10	70	1
Damage type 1 at 3L/4			
9	10	30	1
10	10	50	1
11	10	70	1
Damage type 2 around mid-span			
12	10	30	2
13	10	30	3

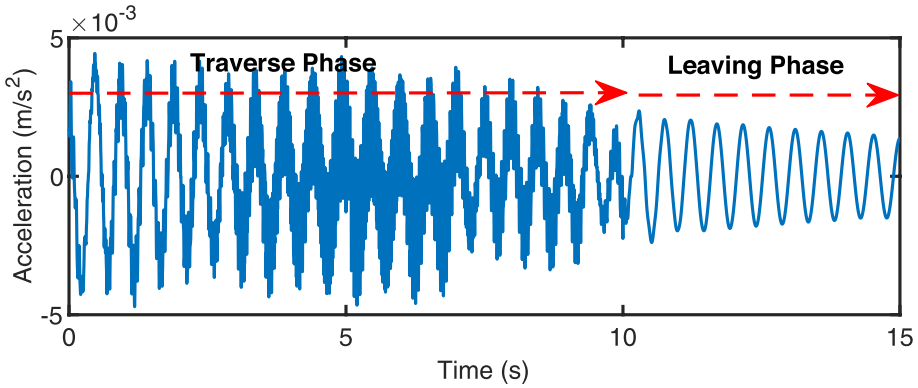

Fig. 5 The forced (traverse phase) and the free (leaving phase) vibration of the baseline simulation response calculated at the bridge mid-span

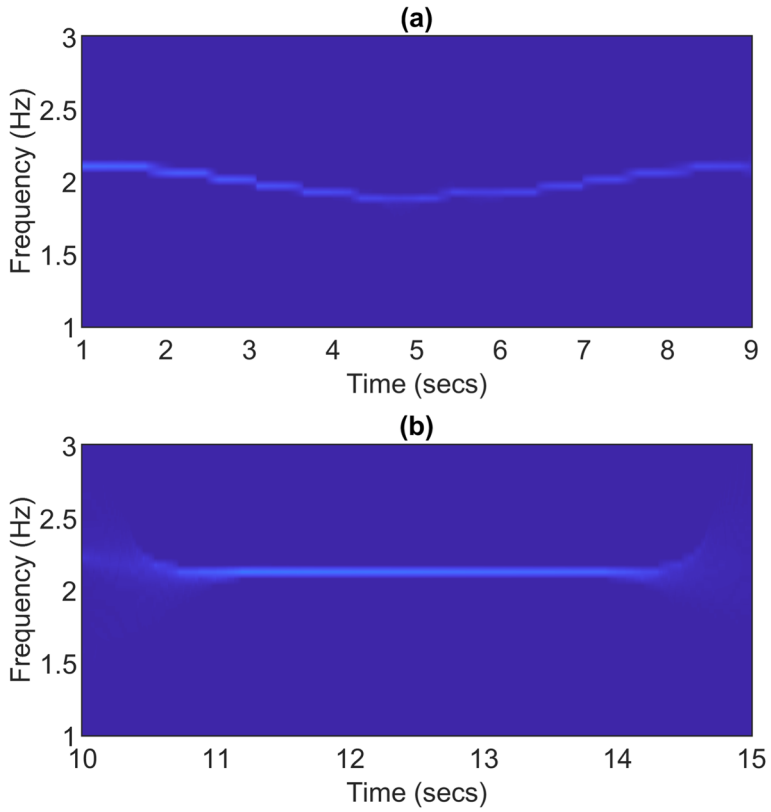

Fig. 6 The instantaneous frequency of the healthy bridge extracted by WSST from (a) the traverse phase, (b) the leaving phase

first step of the proposed approach, as presented in the Section 2.1, is required since the bridge forced and free vibration responses are in practice not recognizable from the time domain signal as presented in Fig. 3. However, this is not the case for the numerical simulation where the entrance, traverse and the leaving phase response are implemented in three different analysis steps. The signal for the entrance phase is a zero acceleration vector which is not plotted and not used for this study. The traverse phase and the leaving phase will be analyzed based on the proposed approach in the Section 2.

The second step is to extract the bridge fundamental frequency by applying WSST to the signal of the leaving phase. Fig. 6 is the time-frequency representation of the leaving phase response. This representation shows the distribution of the energy over the frequency range at each time instance.

It shows the bridge frequency is constant at 2.1 Hz as expected for a stationary signal. WSST is then applied to the traverse phase response to trace back the frequency component of 2.1 Hz during the traverse phase. The time frequency representation of the traverse phase is shown in Fig. 6. The bridge instantaneous frequency as a time-frequency array can be obtained by extracting the frequency ridge. The bridge baseline instantaneous frequency, $\mathcal{F}_b$ is presented in Fig. 7 in blue.

$\mathcal{F}_b$ is presented for the time period 1-9 s instead of 0-10 s. The reason is to avoid signal end effects which might cause disruption of the frequency ridge. It can also be observed that the time frequency array is step-wise rather than continuous due to the limited frequency resolution of the WSST results. $\mathcal{F}_b$ as presented in Fig. 7 displays that the bridge resonance when the vehicle passes the bridge mid-span (t=5 s) is 1.9 Hz. It shows that the operational condition (added mass) has indeed reduced the bridge natural frequency by 9.5%.

4.2 Variable operational condition

Up to this stage, the first test case is performed, and the system baseline frequency variation corresponding to the healthy state of the bridge is provided. It has already been mentioned that the resonances of a VBI system can deviate from the baseline either due to the dynamic interaction between the sub-systems or due to damage. In this section, test cases 2-5 are defined such that the mass, as the operational condition, is changed to 0.5, 1.5, 2, and 2.5 times the value used in the baseline simulation (test case 1). Figure 7 shows the extracted instantaneous frequency for the baseline and variable operational condition test cases.

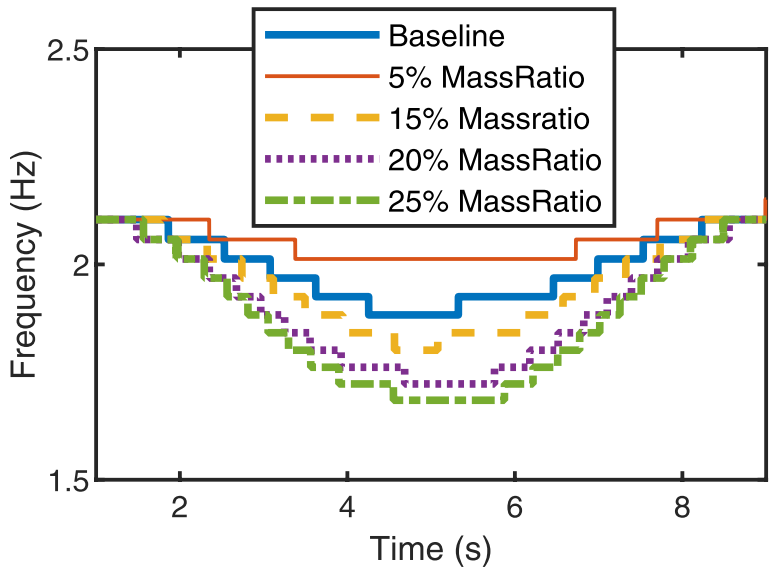

Fig. 7 The instantaneous frequency of the bridge forced response induced by different vehicle mass

It can be clearly seen that the mass change leads to a different system and, subsequently, a different time-frequency content compared to the baseline. Moreover, it can be seen that the curvature of the instantaneous frequency of the systems corresponds to the vehicle mass ratios. In Fig. 7, the top instantaneous frequency (plotted in red) is for the system with the lowest vehicle-bridge mass ratio (5%) and the bottom one (plotted in green) is for the system with the highest vehicle-bridge mass ratio (25%).

For a test case, once the obtained instantaneous frequency, $\mathcal{F}_m$ is different from the baseline instantaneous frequency, $\mathcal{F}_b$ the shape correlation, ρ and the magnitude variation, δ should be investigated. ρ and δ are calculated for $\mathcal{F}_b$ and $\mathcal{F}_m$ for a test case by utilizing Eqs. 4 and 5 respectively. For the variable operational condition test cases (2-5) with the mass ratios of 5%, 15%, 20%, and 25% the shape correlation coefficients are equal to 0.94, 0.98, 0.97, 0.97 respectively and the magnitude variation yielding the values -0.56, 0.35, 0.91 and 1.14 respectively. Apart from test case 2, for test cases 3-5, the shape correlation coefficients are larger than 0.97 and the magnitude variation values are larger than 0.2. For the intact bridge, when the vehicle mass changes $\mathcal{F}_b$ is affected globally as displayed in Fig. 7. Therefore, The magnitude variation which calculates the bounded area between $\mathcal{F}_b$ and $\mathcal{F}_m$ (Eq. 5) becomes a larger value in comparison with a local $\mathcal{F}_b$ deviation like damage. It can be concluded that the high correlation coefficients, $\rho \geq 0.97$ and a relatively large magnitude variation, $\delta \geq 0.2$ imply that the source of the frequency change is the operational condition.

The shape correlation of test case 2 is 0.94 which is lower than the shape correlation coefficients of test cases 3-5 and the magnitude variation is negative. The denominator of Eq. 5 is always a positive value, however, the numerator can be negative or positive depending on $\mathcal{F}_b$ and $\mathcal{F}_m$. For the second test case the mass ratio (5%) is smaller than the mass ratio of the baseline test case (10%). As displayed in (Fig. 7), $\mathcal{F}_m$ for test case 2 appears above the baseline, $\mathcal{F}_b$ and accordingly, the magnitude variation becomes negative. A negative magnitude variation implies a change in operational condition or an increase of the system stiffness which is not expected in the case of damage. Therefore, regarding the 13 test cases of the current study, the source of the baseline deviation for test case with negative magnitude variation is the operational condition.

4.3 Variable damage severity at the bridge mid-span

This section investigates test cases 6-8 corresponding to three damage scenarios. The scenarios are defined such that the bridge mid-span element is damaged with different severity levels. All the steps of the proposed approach are performed, and $\mathcal{F}_m$ for each damage case is presented in Fig. 8.

It can be seen that for the 30%, 50% and 70% damage, $\mathcal{F}_m$ deviates from $\mathcal{F}_b$ around the time when the moving mass crosses the damaged element. The correlation coefficients, ρ for the test cases corresponding to the 30%, 50%, and 70% damage cases are 0.98, 0.92, and 0.90, respectively. $\mathcal{F}_m$ of the first damage case still highly correlates with the baseline due to the small amount of damage. Therefore, the shape correlation is not sufficient to reveal the source of the baseline deviation. The baseline magnitude variation is required. δ for test cases 6-8 are equal to 0.08, 0.30, and 0.48, respectively.

Figure 9 displays the shape correlation and the magnitude variation for all test cases. Test case 6-8 are displayed with red marker in Fig. 9. In Fig. 9 different test scenarios

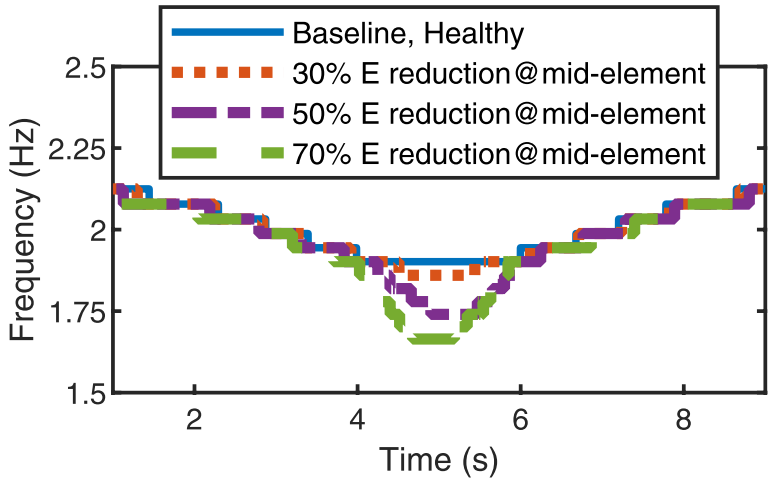

Fig. 8 The bridge baseline $\mathcal{F}_b$ and $\mathcal{F}_m$s for the bridge having damage at $L/2$ caused by various damage severity levels

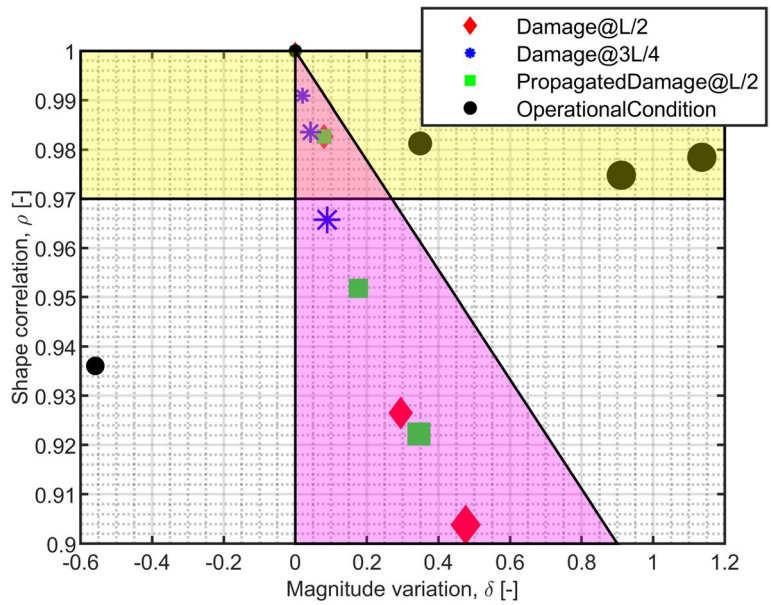

Fig. 9 The magnitude variation and the shape correlation for the damaged test cases and the variable operational conditions test cases

are displayed in different colors, and the marker size corresponds to the damage size. It can be seen that by increasing damage, the shape correlation decreases, and the magnitude variation increases. However, the scale of the increase in magnitude variation for the damaged cases (test cases 6-8) is different from those for variable operational conditions (test cases 1-5). A small magnitude variation implies a local variation like damage. In contrast, a relatively large magnitude variation, $\delta \geq 0.2$ is caused by the operational condition where the baseline instantaneous frequency changes along the entire bridge span. For example, consider test case 3, where the vehicle mass is changed, and test case 6, when the bridge mid-span element is damaged. For both test cases, the shape correlation value is the same and equal to 0.98. However, the magnitude variation for test

case 2, where the vehicle mass is changed, is 0.35, and it is much larger than 0.08, the magnitude variation of test case 6, where the bridge is damaged at mid-span. Therefore, for the cases where the shape correlation, ρ is greater or equal to 0.97 the magnitude variation, δ is the determining factor. For the damage cases, by increasing the damage, ρ decreases and δ does not strongly increase as displayed by the steep trend line with pink background in Fig. 9. However, for the healthy bridge by increasing the operational condition, ρ remains high ($\rho \geq 0.97$) and δ continues to increase ($\delta \geq 0.2$) displayed by the near horizontal trend line with yellow background in Fig. 9. For a case with high shape correlation ($\rho >= 0.97$) and small magnitude variation ($\delta < 0.2$), where the two background colors overlap in Fig. 9, the method cannot distinguish if the baseline deviation is caused by change in operational condition or damaged. That is the limit of the sensitivity of the proposed method.

4.4 Variable damage severity at the bridge three-quarter

The objective of this part is to investigate the performance of the proposed damage detection technique for the cases where the damage location is far from the sensor node, which in this case is assumed to be located at mid-span. Test cases 9-11 are investigated in this section, where the damage size and severity are similar to the previous section. The only difference is that the damage is relocated to $3L/4$ of the bridge span while the measurement point of the vibration is at the bridge mid-span. The damage location is 12.5 m (25% of the bridge span) away from the measurement point. The instantaneous frequency corresponding to each damage severity is extracted and displayed in Fig. 10. The correlation coefficients corresponding to the 30%, 50% and 70% damage at $3L/4$ are equal to 0.99, 0.98 and 0.96. The correlation coefficients for the damage cases at the three-quarter span length of the bridge are higher than the shape correlation for the damage cases at the bridge mid-span. It is explained by the distance between damage and observation point and by the fact that the change of the baseline frequency is already smaller at that location. Since the first vibration mode of the bridge has its maximum deflection at the mid-span, the mid-span will also be the most sensitive place to capture

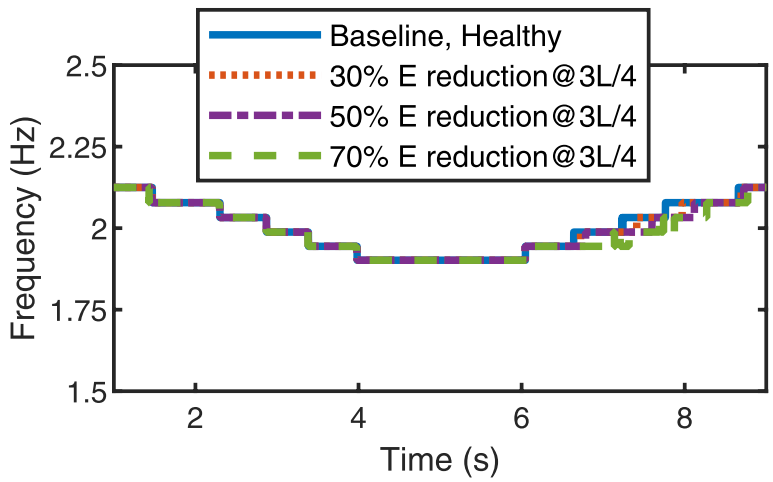

Fig. 10 The bridge baseline $\mathcal{F}_b$ and $\mathcal{F}_m$s for the bridge having damage at $3L/4$ caused by various damage severity levels

the dynamic variation properties. The performance of the method can be improved in the future by adding more sensors.

The magnitude variation values for test cases 9-11 are 0.02, 0.04, and 0.09, where the small magnitude variation values imply the local variation like damage. For example, consider test case 3 and 10, where the shape correlation for both is 0.98. However, the magnitude variation of test case 3 corresponding to the change of operational condition is 0.35, which is much larger than 0.04, the magnitude variation of the damaged bridge. Therefore, the baseline frequency deviation is caused by damage when a combination of a decrease in correlation coefficient and a limited magnitude variation occurs. It can be concluded that even for the cases where the damage is relatively small and far from the bridge mid-span, the proposed method can still properly detect the different damage severity levels.

4.5 Variable damage length at the bridge mid-span

This final subsection aims at investigating an extended damage scenario around mid-span. To do so, the 30% stiffness reduction at the mid-element is extended to two and three adjacent elements. For each case, the instantaneous frequency is plotted in Fig. 11.

The results of test cases for the propagated damage at the bridge mid-span are plotted in green in Fig. 9. The shape correlation coefficient values for test cases 6,12, and 13 corresponding to the bridge having one, two, and three damaged elements at the bridge mid-span are 0.98, 0.95, and 0.92. The magnitude variation values for test cases 6, 12, and 13 are equal to 0.08, 0.18, and 0.35. For test cases 12 and 13, the shape correlation is smaller than 0.97, implying that the baseline instantaneous frequency deviates due to damage. For test case 6, where the shape correlation is high, 0.98, the magnitude variation is 0.08, and it is smaller than 0.2. Therefore it represents a damaged bridge.

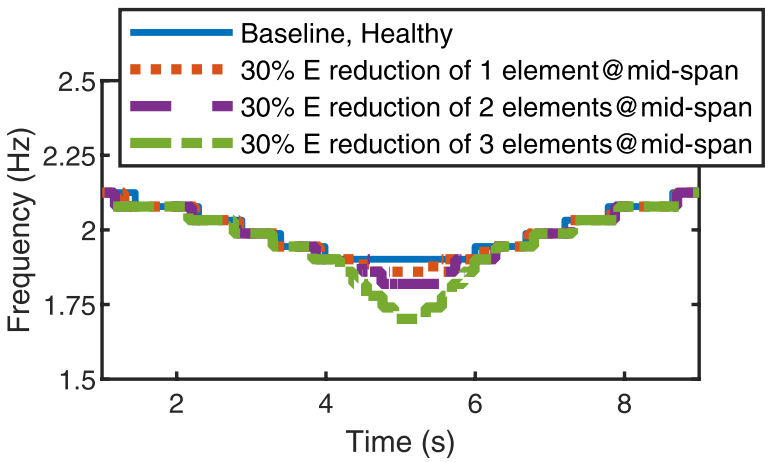

Fig. 11 The bridge baseline $\mathcal{F}_b$ and $\mathcal{F}_m$s for the bridge having various sizes of damage around $L/2$

5 Summary

The results of the two proposed features; the shape correlation (ρ) and the magnitude variation (δ) between the baseline ($\mathcal{F}_b$) and a measured instantaneous frequency ($\mathcal{F}_m$ for test cases 2-13 are summarized in Table 3. Figure 9 shows the magnitude variation versus the shape correlation for all test cases. It can be seen that the pattern of the results of the damaged cases is different from the cases with varying operational condition. The vehicles with different masses are displayed with the black circles where the increasing size of the marker implements the increase of the mass ratio from 10% to 15%, 20% and 25%. By increasing the mass ratio, the magnitude variation increases where the shape correlations are about 0.98. Regarding the damage cases, it can be seen that by increasing damage severity or length, the shape correlation coefficient decreases, whereas, the magnitude variation remains relatively low. Moreover, the shape correlation coefficients for the damage cases at the three-quarters length of the bridge are higher than the shape correlations coefficients for the same amount of damage but at the bridge mid-span.

6 Performance of the wSST versus fFT and cWT

A comparison between the proposed approach and the conventional technique, using the FFT of the leaving phase response, is performed to demonstrate the first three axioms of the proposed method addressed in the 1. Conventionally, the change in the natural frequencies of the bridge obtained from the free vibration response is used as an indication of damage. Figure 12b shows that the bridge natural frequency does not change for different vehicle masses, whereas a slight frequency reduction for the most severe damage case can be seen in Fig. 12d.

Table 3 The healthy and damage scenarios that have been investigated numerically

Test case	Vehicle-bridge mass ratio (%)	Stiffness reduction (%)	Damaged element (No.)	ρ	δ
Baseline simulation					
1	10	-	-	1	0
Variable operational condition					
2	5	-	-	0.94	-0.56
3	15	-	-	0.98	0.35
4	20	-	-	0.97	0.91
5	25	-	-	0.97	1.14
Damage type 1 at L/2					
6	10	30	1	0.98	0.08
7	10	50	1	0.92	0.30
8	10	70	1	0.90	0.48
Damage type 1 at 3L/4					
9	10	30	1	0.99	0.02
10	10	50	1	0.98	0.04
11	10	70	1	0.96	0.09
Damage type 2 around mid-span					
12	10	30	2	0.95	0.18
13	10	30	3	0.92	0.35

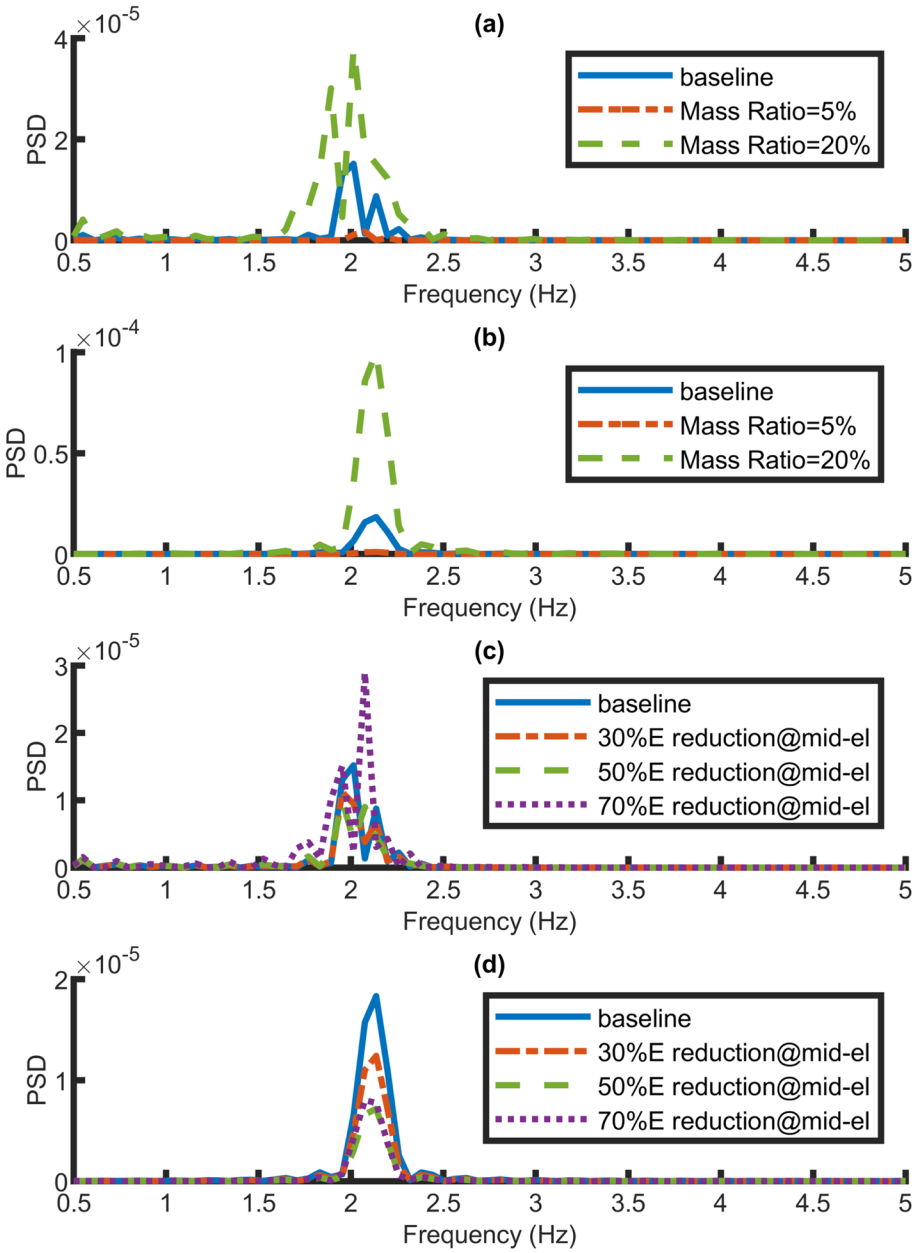

Fig. 12 The PSD of a) the traverse phase for the variable operational conditions, b) the leaving phase response for variable operational conditions, c) the traverse phase in case of damage and, d) the leaving phase in case of damage

This observation verifies the first axiom of the proposed method, stating that the bridge free vibration mainly reflects the global dynamic properties. Moreover, Fig. 12b and d show that the different cases yield a clear difference in the magnitude of the Power Spectral Density (PSD). However, this does not distinguish the effects of the damage and operational conditions. Figure 12a and c show the frequency content of the traverse phase for variable operational conditions and the damaged cases, respectively.

The figures show that the traverse phase response is much more sensitive than the free vibration response to both sources since the change of the baseline peak frequencies is

more visible in the traverse phase, and this observation verifies the third axiom of the proposed method. However, using only the frequency content of the VBI response is not adequate and reliable since the traverse phase response represents a non-stationary response which means that the frequency content of the signal changes over time. Therefore, looking at the frequency content and interpreting the changes of the peak frequencies is not informative to learn about the changes caused by time-dependent and local events such as damage. This observation verifies the second axiom, which utilizes the Instantaneous Frequency of the VBI system instead of the resonance frequency.

As addressed in the last axiom of the proposed method, a high-resolution time-frequency analysis technique is required to extract the system instantaneous frequency, as the enabler, as accurately as possible. Therefore, the performance of the WSST is compared with CWT as the widely used time-frequency technique. To provide consistency and re-producibility of the results, Matlab functions with default settings are utilized for both techniques. Figure 13 shows the instantaneous frequency extracted by the WSST and CWT for the different conditions of the bridge. Figure 13a shows the instantaneous frequency of the healthy bridge extracted by WSST and CWT in red and black, respectively.

It can be seen that the resolution of the extracted frequency ridge by the CWT is much lower than the IF extracted by WSST. The fundamental difference between the CWT and WSST is about the frequency resolution and the interested readers are referred to (Mostafa et al. 2021). Regarding the damaged bridge Fig. 8 has already shown that the shape of the bridge instantaneous frequency changes due to 30% and 50% damage at the bridge mid-span element. However, it can be seen in Fig. 13b and c that the frequency ridge extracted by CWT for these two damage cases are nearly similar. Therefore, it can be concluded that WSST outperforms CWT to detect local events like damage.

7 Performance of the wSST with noise

Noise is the main difference between a measured bridge response and the corresponding simulated response. Noise is a determining factor that challenges the damage detection techniques based on finding response singularities and wavelet coefficients. However, those techniques are verified numerically or experimentally in a controlled laboratory environment. When the damage-sensitive feature is defined based on the signal disruption once damage occurs, the performance of the techniques in distinguishing the damage from the noise is questionable. However, it is not the case for the current study's proposed approach, where the VBI system's instantaneous frequency, which is in a low frequency range, is utilized as the damage-sensitive feature. White noise corresponding to the signal-to-noise ratio (SNR) of Boyne viaduct (as the case study) equal to 10 is added to the simulated bridge response to verify the performance of the proposed approach. Figure 14 presents the bridge instantaneous frequency extracted from the simulated signal without noise in color and with noise in black. It can be seen that the noise has not affected the bridge instantaneous frequency. For further investigation, higher noise levels with lower SNR are added to the response. Three SNR levels, 10, 5, and 0.1 are added to the bridge simulated response in healthy and damaged conditions. To evaluate the influence of the added noise, the shape correlation coefficient between the bridge instantaneous frequency extracted

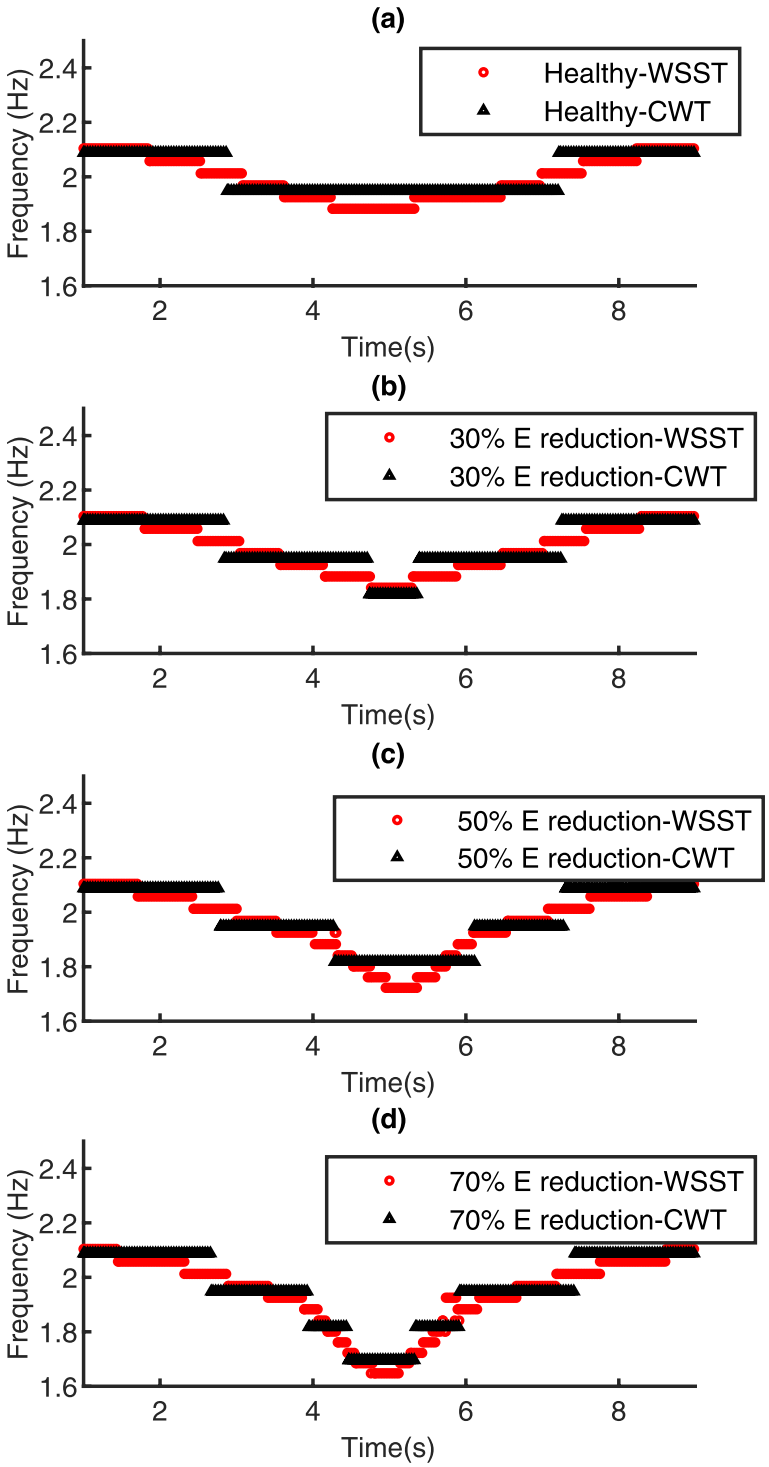

Fig. 13 The bridge instantaneous frequency extracted by WSST and CWT for a) the healthy bridge, an the damaged bridge with b) 30% c) 50% d) 70% E reduction at the mid-span element

from the traverse phase response with the different noise levels is calculated and presented in Fig. 15. It can be seen that the correlation coefficients corresponding to the three noise levels and the four bridge conditions are similar and not dispersed, which

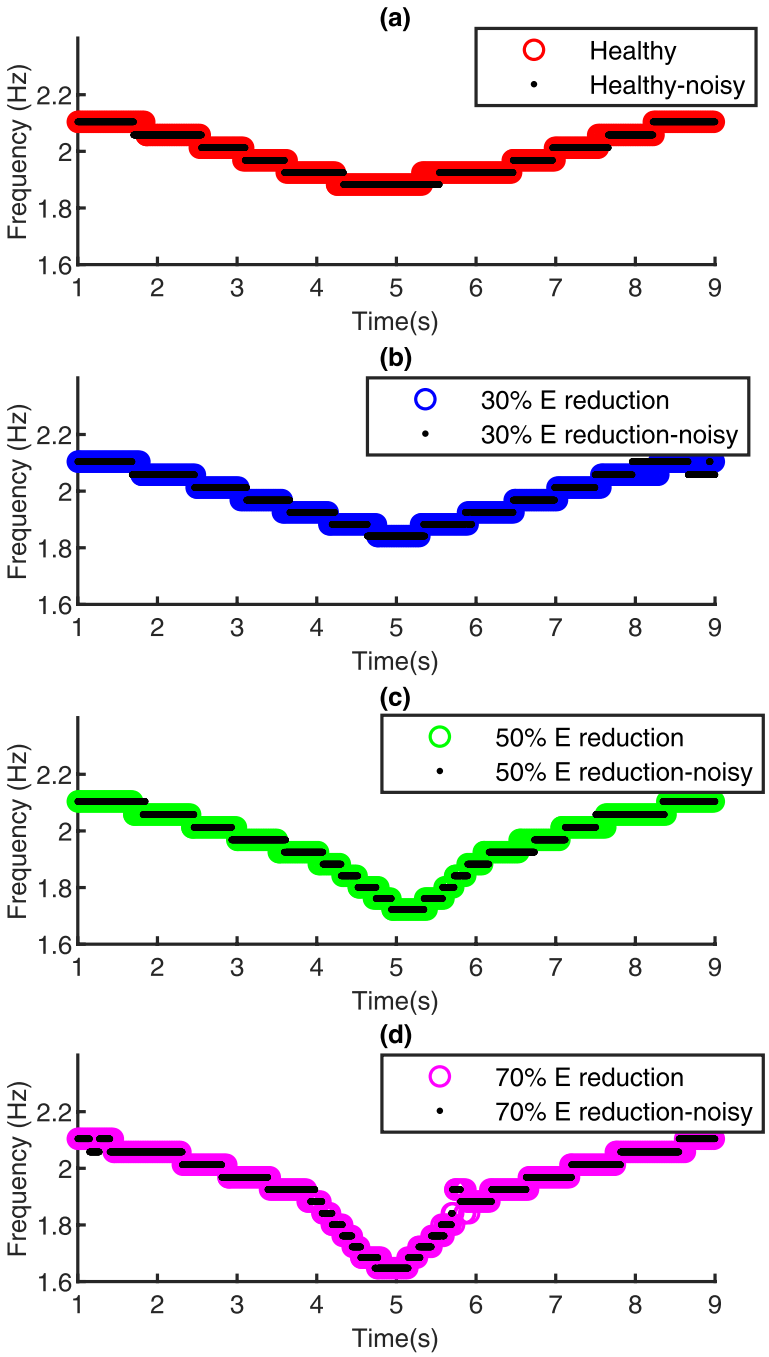

Fig. 14 The bridge instantaneous frequency extracted from the simulated signal with and without noise for a) the healthy bridge, an the damaged bridge with b) 30% c) 50% d) 70% E reduction at the mid-span element

verifies the robustness of the WSST concerning noise. Therefore, it can be concluded that the proposed damage detection technique is not sensitive to noise.

It should be noted that the proposed method has been applied to a series of simulated signals for which the results are promising. The combination of the variable operational

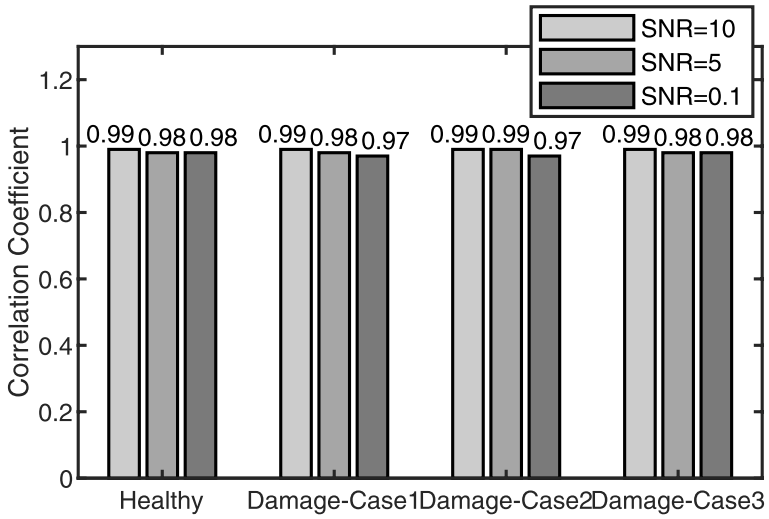

Fig. 15 The correlation coefficient between the bridge baseline instantaneous frequency extracted from the bridge simulated signals without noise and with noise

condition and damage will be considered in future work. However, based on the current study results, it is believed that for the case of the combined variables, the proposed method can distinguish the variable operational condition and the damage, although the proposed damage index needs to be adapted to the new situation in the future work.

8 Conclusion

A method has been proposed that extends the traditional damage detection techniques based on the bridge natural frequencies extracted from the bridge free vibration. This study presented a concept for damage detection in (railway) bridges based on the instantaneous frequency analysis of the bridge forced and free vibration responses. Within this concept, based on the bridge natural frequency extracted from the bridge free vibration f_b, a healthy baseline ($\mathcal{F}_b$) was obtained by applying the Wavelet Synchrosqueezed transform (WSST) to the bridge forced vibration response. The objective was to understand how well WSST is capable of filtering information related to damage and separate it other sources of variation in the signal. The shape correlation ρ and the magnitude variation δ proposed to distinguish the global and the local deviation of the bridge baseline instantaneous frequency induced by variable operational conditions and damage, respectively. Finally, if the source of the baseline deviation is damage, then the magnitude variation, δ can be used as a damage index. The proposed damage index is a preliminary step towards damage quantification. Furthermore, for the damaged test cases, the local deviation of the baseline instantaneous frequency around the damage location shows the potential of the proposed method for damage localization. However, damage localization is out of the scope of the current study. Including the baseline simulation, 13 test cases have been analyzed to verify the performance of the proposed method. The results show that;

- Information on the time-variant resonance frequency is highly valuable and more informative than the natural frequency, extracted from the bridge free-decay, to detect local events like damage.
- The instantaneous frequency of the vehicle-bridge interaction response obtained with the WSST outperforms the CWT due to the higher resolution for the lower frequency range.
- The bridge baseline instantaneous frequency deviates due to damage or operational condition. The damage can be distinguished from the variation of the operational condition using the combination of the shape correlation coefficients (ρ) and the magnitude variation (δ).
- For damaged bridge, the magnitude variation (δ) is a first step towards quantification of the damage.

The current study investigated a moving mass model. A next step is to perform an experimental study to verify the findings. Moreover, future work will extend the model to more realistic moving masses with a dual suspension system and more complex yet more realistic dynamic behavior.

Abbreviations

VBI	Vehicle Bridge Interaction
IF	Instantaneous Frequency
DI	Damage Index
FFT	Fast Fourier Transform
CWT	Continuous Wavelet Transform
WSST	Wavelet Synchrosqueezed Transform
EMD	Empirical Mode Decomposition
EEMD	Ensemble Empirical Mode Decomposition
MFI	Moving Force Identification
OMA	Output-only Modal Analysis
DSF	damage Sensitive Feature
IMF	Intrinsic Mode Function
PSD	Power Spectral Density

Acknowledgements
This study has been performed as part of the DESTination RAIL project – Decision Support Tool for Rail Infrastructure Managers.

Authors' contributions
N.M. mainly contributed to the research and numerical studies, T.T., R.L. and D.D. mainly contributed as technical leading and support. The author(s) read and approved the final manuscript.

Authors' information
N.Mostafa; a PhD candidate at university of Twente. D. Di Maio; assistant professor at university of Twente. R. Loendersloot; associated professor at university of Twente. T. Tinga; full professor at university of Twente.

Funding
the DESTination RAIL project has received funding from the European Union's Horizon 2020 research and innovation program under grant agreement No 636285.

Availability of data and materials
The University of Twente is the owner of the research data. The research data can be available considering the data management policy of the University of Twente.

Declarations

Ethics approval and consent to participate
Not applicable.

Consent for publication
Not applicable.

Competing interests
The authors have no competing interest.

Received: 14 June 2022 Accepted: 8 August 2022
Published online: 01 October 2022

References

Aied, H, Gonzalez A, Cantero D (2016) Identification of sudden stiffness changes in the acceleration response of a bridge to moving loads using ensemble empirical mode decomposition. Mech Syst Signal Process 66-67:314–338. https://doi.org/10.1016/j.ymssp.2015.05.027.

Babajanian Bisheh, H, Ghodrati Amiri G, Nekooei M, Darvishan E (2020) Damage detection of a cable-stayed bridge based on combining effective intrinsic mode functions of empirical mode decomposition using the feature selection technique. Inverse Probl Sci Eng 29(6):861–881. https://doi.org/10.1080/17415977.2020.1814280.

Cantero, D, Ülker-Kaustell M, Karoumi R (2016) Time–frequency analysis of railway bridge response in forced vibration. Mech Syst Signal Process 76-77:518–530. https://doi.org/10.1016/j.ymssp.2016.01.016.

Chang, K-C, Kim C-W (2016) Modal-parameter identification and vibration-based damage detection of a damaged steel truss bridge. Eng Struct 122:156–173. https://doi.org/10.1016/j.engstruct.2016.04.057.

Chen, JUN (2009) Application of empirical mode decomposition in structural health monitoring: Some experience. Adv Adapt Data Anal 01(04):601–621. https://doi.org/10.1142/s1793536909000321.

Comanducci, G, Magalhaes F, Ubertini F, Cunha A (2016) On vibration-based damage detection by multivariate statistical techniques: Application to a long-span arch bridge. Struct Health Monitoring-an Int J 15(5):505–524. https://doi.org/10.1177/1475921716650630.

Connolly, DP, Kouroussis G, Laghrouche O, Ho CL, Forde MC (2015) Benchmarking railway vibrations – track, vehicle, ground and building effects. Constr Build Mater 92:64–81. https://doi.org/10.1016/j.conbuildmat.2014.07.042.

Connolly L, Prendergast L, Mostafa N, Loendersloot R (2017) Report on assessment of bridges. Report. http://www.destinationrail.eu/ajax/DownloadHandler.php?file=2135

Daubechies, I, Maes S (1996) A nonlinear squeezing of the continuous wavelet transform based on auditory nerve models. 1st edition edn.. CRC Press, New York. Chap. 20. https://doi.org/10.1201/9780203734032.

Daubechies, I, Lu JF, Wu HT (2011) Synchrosqueezed wavelet transforms: An empirical mode decomposition-like tool. Appl Comput Harmon Anal 30(2):243–261. https://doi.org/10.1016/j.acha.2010.08.002.

Dilena, M, Limongelli MP, Morassi A (2015) Damage localization in bridges via the frf interpolation method. Mech Syst Signal Process 52-53:162–180. https://doi.org/10.1016/j.ymssp.2014.08.014.

Doebling SW, Farrar CR, Prime MB (1998) A summary review of vibration-based damage identification methods. Shock Vib Dig. https://doi.org/10.1177/058310249803000201

Farahani, RV, Penumadu D (2016) Damage identification of a full-scale five-girder bridge using time-series analysis of vibration data. Eng Struct 115:129–139. https://doi.org/10.1016/j.engstruct.2016.02.008.

Friswell, MI (2007) Damage identification using inverse methods. Philos Trans A Math Phys Eng Sci 365(1851):393–410. https://doi.org/10.1098/rsta.2006.1930.

Gonzalez, A, Hester D (2013) An investigation into the acceleration response of a damaged beam-type structure to a moving force. J Sound Vib. https://doi.org/10.1016/j.jsv.2013.01.024.

He, W-Y, Zhu S (2016) Moving load-induced response of damaged beam and its application in damage localization. J Vib Control 22(16):3601–3617. https://doi.org/10.1177/1077546314564587.

He, XH, Hua XG, Chen ZQ, Huang FL (2011) Emd-based random decrement technique for modal parameter identification of an existing railway bridge. Eng Struct 33(4):1348–1356. https://doi.org/10.1016/j.engstruct.2011.01.012.

Hester, D, Gonzalez A (2012) A wavelet-based damage detection algorithm based on bridge acceleration response to a vehicle. Mech Syst Signal Process 28:145–166. https://doi.org/10.1016/j.ymssp.2011.06.007.

Zhang, W, Li J, Hao H, Ma H (2017) Damage detection in bridge structures under moving loads with phase trajectory change of multi-type vibration measurements. Mech Syst Signal Process 87:410–425. https://doi.org/10.1016/j.ymssp.2016.10.035.

Huseynov, F, Kim C, Obrien EJ, Brownjohn JMW, Hester D, Chang KC (2020) Bridge damage detection using rotation measurements – experimental validation. Mech Syst Signal Process 135. https://doi.org/10.1016/j.ymssp.2019.106380.

Zhu, XQ, Law SS (2006) Wavelet-based crack identification of bridge beam from operational deflection time history. Int J Solids Struct 43(7-8):2299–2317. https://doi.org/10.1016/j.ijsolstr.2005.07.024.

Khorram, A, Rezaeian M, Bakhtiari-Nejad F (2013) Multiple cracks detection in a beam subjected to a moving load using wavelet analysis combined with factorial design. Eur J Mech A/Solids 40:97–113. https://doi.org/10.1016/j.euromechsol.2012.12.012.

Kirch, W (2008) Encyclopedia of Public Health. Springer. https://doi.org/10.1007/978-1-4020-5614-7_2569.

Li, J, Law SS, Hao H (2013) Improved damage identification in bridge structures subject to moving loads: Numerical and experimental studies. Int J Mech Sci 74:99–111. https://doi.org/10.1016/j.ijmecsci.2013.05.002.

Li, D, Wang Y, Yan W-J, Ren W-X (2020) Acoustic emission wave classification for rail crack monitoring based on synchrosqueezed wavelet transform and multi-branch convolutional neural network. Struct Health Monit 20(4):1563–1582. https://doi.org/10.1177/1475921720922797.

Malekjafarian, A, Golpayegani F, Moloney C, Clarke S (2019) A machine learning approach to bridge-damage detection using responses measured on a passing vehicle. Sensors (Basel) 19(18). https://doi.org/10.3390/s19184035.

Lu, Y, Mao L, Woodward P (2012) Frequency characteristics of railway bridge response to moving trains with consideration of train mass. Eng Struct 42:9–22. https://doi.org/10.1016/j.engstruct.2012.04.007.

Mostafa, N, Di Maio D, Loendersloot R, Tinga T (2021) Extracting the time-dependent resonances of a vehicle–bridge interacting system by wavelet synchrosqueezed transform. Struct Control Health Monit. https://doi.org/10.1002/stc.2833.
Mahmoud, MA (2001) Effect of cracks on the dynamic response of a simple beam subject to a moving load. Proc Inst Mech Eng F J Rail Rapid Transit 215(3):207–215. https://doi.org/10.1243/0954409011531521.
Meredith, J, Gonzalez A, Hester D (2012) Empirical mode decomposition of the acceleration response of a prismatic beam subject to a moving load to identify multiple damage locations. Shock Vib 19(5):845–856. https://doi.org/10.3233/Sav-2012-0693.
Moughty, JJ, Casas JR (2017) A state of the art review of modal-based damage detection in bridges: Development, challenges, and solutions. Appl Sci-Basel 7(5). https://doi.org/10.3390/app7050510.
Nguyen, KV (2013) Comparison studies of open and breathing crack detections of a beam-like bridge subjected to a moving vehicle. Eng Struct 51:306–314. https://doi.org/10.1016/j.engstruct.2013.01.018.
Obrien, EJ, McGetrick PJ, Gonzalez A (2014) A drive-by inspection system via vehicle moving force identification. Smart Struct Syst 13(5):821–848. https://doi.org/10.12989/sss.2014.13.5.821.
Obrien, E, Carey C, Keenahan J (2015) Bridge damage detection using ambient traffic and moving force identification. Struct Control Health Monit 22(12):1396–1407. https://doi.org/10.1002/stc.1749.
Ojeda AP (2012) Matlab implementation of an operational modal analysis technique for vibration-based structural health monitoring. Master Sci. http://hdl.handle.net/1721.1/74412. Accessed 2012
Pakrashi, V, Basu B, O' Connor A (2007) Structural damage detection and calibration using a wavelet–kurtosis technique. Eng Struct 29(9):2097–2108. https://doi.org/10.1016/j.engstruct.2006.10.013.
Pakrashi, V, O'Connor A, Basu B (2009) A bridge-vehicle interaction based experimental investigation of damage evolution. Struct Health Monit Int J 9(4):285–296. https://doi.org/10.1177/1475921709352147.
Rainieri, C, Fabbrocino G (2014) Operational Modal Analysis of Civil Engineering Structures. https://doi.org/10.1007/978-1-4939-0767-0.
Roveri, N, Carcaterra A (2012) Damage detection in structures under traveling loads by hilbert-huang transform. Mech Syst Signal Process 28:128–144. https://doi.org/10.1016/j.ymssp.2011.06.018.
Santos, A, Figueiredo E, Silva M, Santos R, Sales C, Costa JCWA (2017) Genetic-based em algorithm to improve the robustness of gaussian mixture models for damage detection in bridges. Struct Control Health Monit 24(3). https://doi.org/10.1002/stc.1886.
Saleeb, AF, Kumar A (2011) Automated finite element analysis of complex dynamics of primary system traversed by oscillatory subsystem. Comput Methods Eng Sci Mech 12(4):184–202. https://doi.org/10.1080/15502287.2011.580830.
Silva, M, Santos A, Figueiredo E, Santos R, Sales C, Costa JCWA (2016) A novel unsupervised approach based on a genetic algorithm for structural damage detection in bridges. Eng Appl Artif Intell 52:168–180. https://doi.org/10.1016/j.engappai.2016.03.002.
Sun, L, Shang Z, Xia Y, Bhowmick S, Nagarajaiah S (2020) Review of bridge structural health monitoring aided by big data and artificial intelligence: From condition assessment to damage detection. J Struct Eng 146(5). https://doi.org/10.1061/(asce)st.1943-541x.0002535.
Yu, L, Chan THT (2007) Recent research on identification of moving loads on bridges. J Sound Vib 305(1-2):3–21. https://doi.org/10.1016/j.jsv.2007.03.057.
Yu, Z, Xia H, Goicolea JM, Xia C (2016) Bridge damage identification from moving load induced deflection based on wavelet transform and lipschitz exponent. Int J Struct Stab Dyn 16(05). https://doi.org/10.1142/s0219455415500030.
Zhai, W, Sun X (2008) A detailed model for investigating vertical interaction between railway vehicle and track. Veh Syst Dyn 23(sup1):603–615. https://doi.org/10.1080/00423119308969544.
Zhai, W, Han Z, Chen Z, Ling L, Zhu S (2019) Train–track–bridge dynamic interaction: a state-of-the-art review. Veh Syst Dyn 57(7):984–1027. https://doi.org/10.1080/00423114.2019.1605085.
Zhang, WW, Geng J, Zhao ZL, Wang ZH (2013) Numerical studies on wavelet-based crack detection based on velocity response of a beam subjected to moving load. Damage Assess Struct X, Pts 1 2 569-570:854. https://doi.org/10.4028/www.scientific.net/KEM.569-570.854.
Zhang L, Brincker R (2005) An Overview of Operational Modal Analysis: Major Development and Issues. In: Brincker R, Møller N (eds) Proceedings of the 1st International Operational Modal Analysis Conference, April 26-27, 2005, Copenhagen, Denmark. Aalborg Universitet, pp 179–190

Publisher's Note